Imaging Proton Transfer and Dihalide Formation Pathways in Reactions of F⁻ + CH₃I

Eduardo Carrascosa,[†] Tim Michaelsen,[†] Martin Stei,[†] Björn Bastian,[†] Jennifer Meyer,[†] Jochen Mikosch,[‡] and Roland Wester*,[†]

[†]Institut für Ionenphysik und Angewandte Physik, Universität Innsbruck, 6020 Innsbruck, Austria
[‡]Max-Born-Institut für Nichtlineare Optik, 12489 Berlin, Germany

ABSTRACT: Ion–molecule reactions of the type $X^- + CH_3Y$ are commonly assumed to produce Y^- through bimolecular nucleophilic substitution (S_N2). Beyond this reaction, additional reaction products have been observed throughout the last decades and have been ascribed to different entrance channel geometries differing from the commonly assumed collinear approach. We have performed a crossed beam velocity map imaging experiment on the $F^- + CH_3I$ reaction at different relative collision energies between 0.4 and 2.9 eV. We find three additional channels competing with nucleophilic substitution at high energies. Experimental branching ratios and angle- and energy differential cross sections are presented for each product channel. The proton transfer product CH_2I^- is the main reaction channel, which competes with nucleophilic substitution up to 2.9 eV relative collision energy. At this level, the second additional channel, the formation of IF^- via halogen abstraction, becomes more efficient. In addition, we present the first evidence for an $[FHI]^-$ product ion. This $[FHI]^-$ product ion is present only for a narrow range of collision energies, indicating possible dissociation at high energies. All three products show a similar trend with respect to their velocity- and scattering angle distributions, with isotropic scattering and forward scattering of the product ions occurring at low and high energies, respectively. Reactions leading to all three reaction channels present a considerable amount of energy partitioning in product internal excitation. The internally excited fraction shows a collision energy dependence only for CH_2I^-. A similar trend is observed for the isoelectronic $OH^- + CH_3I$ system. The comparison of our experimental data at 1.55 eV collision energy with a recent theoretical calculation for the same system shows a slightly higher fraction of internal excitation than predicted, which is, however, compatible within the experimental accuracy.
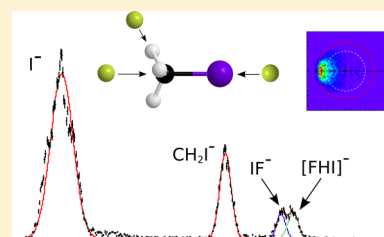
INTRODUCTION

The bimolecular nucleophilic substitution (S_N2) reaction is one of the fundamental reaction types in physical organic chemistry and has been the subject of extensive experimental and theoretical studies for more than a century.[1−9] The simplest representation of a nucleophilic substitution consists of a methyl halide reacting with an atomic halogen anion:

$$X^- + CH_3Y \rightarrow CH_3X + Y^- \quad (X, Y = F, Cl, Br, I) \tag{1}$$

The energetics of nucleophilic substitution in the gas phase has been studied very precisely for decades and is described by a minimum energy pathway consisting of two potential energy wells separated by a potential energy barrier that corresponds to the transition state.[3,10] The barrier has been the subject of many studies because it acts as a hindrance to product formation. This hindrance occurs at thermal conditions even for submerged barriers due to the low density of states at this transition state. The three main steps used to describe this reaction are the following: first, the approach of the nucleophile and the formation of an ion-dipole prereaction complex; second, the well-known Walden inversion of the CH_3 umbrella, which corresponds to the central transition state; and lastly, the formation of a second postreaction ion–dipole complex followed by the exit of the leaving halogen atom after the

C−Y bond cleavage. In the classical textbook picture, the described mechanism occurs in a collinear way, and the mentioned ion-dipole complexes all possess C_{3v} symmetry. This mechanism is commonly called backside attack of the nucleophile.

In the last decades, the combination of new experimental techniques[11,12] and the development of high level ab initio methods and quasiclassical trajectory calculations[13−15] have led to a better understanding of the atomic-level mechanisms that govern these reactions.[16] Due to this fruitful collaboration, the effect of the nucleophile, of the leaving group, and of solvation on nucleophilic substitution have been analyzed,[17,18] and even nonintuitive reaction mechanisms have been unraveled.[19−21]

Many of these newly discovered mechanisms imply alternative entrance channel geometries beyond the collinear approach. Among them, a front-side mechanism where the nucleophile attacks the CH_3I molecule from the iodine side and directly replaces the leaving group without CH_3 inversion has

been proposed[22] and well-characterized.[14,23] Also a hydrogen-bonded prereaction complex where the anion points to a C−H bond axis of the methyl halide has been established.[24,25] These alternative entrance channel geometries not only change the kinematics and dynamics of the reaction producing the mechanisms mentioned above but also can lead to completely different products competing with nucleophilic substitution in these ion−molecule reactive systems, e.g.:

$$X^- + CH_3Y \rightarrow XH + CH_2Y^- \quad (2)$$

$$X^- + CH_3Y \rightarrow CH_3 + XY^- \quad (3)$$
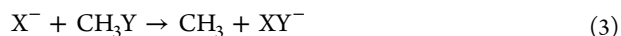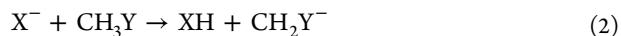
Reaction (2) consists of a proton abstraction mechanism induced by an XH-bonded prereaction complex, whereas reaction (3) produces a dihalide anion through a halogen abstraction mechanism. These reaction products have been predicted and experimentally observed many years ago.[22,26,27] Cross sections have been obtained as a function of relative energy for several $X^- + CH_3Y$ systems.[28,29] Theoretical studies have focused mainly on the reaction type (2), investigating the properties of the $[X−HCH_2Y]^-$ prereaction complex.[24,25,30] The contribution of the proton transfer channel has been shown to strongly depend on the proton affinity of the nucleophile.[21] The halogen abstraction mechanism, which produces a dihalide anion, has only seen little attention up to now.[28,31]

This article focuses on the $F^- + CH_3I$ reaction, a system which has been extensively studied in the last years, both experimentally and theoretically: Recent electronic structure calculations have revealed an energetically stable $[F−HCH_2I]^-$ ion dipole complex,[24,32] which has been shown to be consistent with a hydrogen-bonded complex in terms of bond length, vibrational frequencies, Mulliken charges, and so on.[30] Its geometry is connected with the collinear prereaction complex through a very small potential energy barrier. The $[F−HCH_2I]^-$ complex can evolve into both proton transfer (CH_2I^-) and nucleophilic substitution (I^-) and is therefore a key stationary point of this system. This entrance channel structure not only drastically changes the standard direct rebound dynamics[33,34] but also favors the formation of products different from nucleophilic substitution.

In order to shed more light onto the particularities of these alternative pathways, we present experimental angle- and energy differential cross sections for the products of reactions (2) and (3) in the $F^- + CH_3I$ system. Additionally, we report on the first observation of a third product, $[FHI]^-$, and we discuss possible pathways along the reaction coordinate that might lead to formation of this species. The paper is organized as follows: The first section comprises a brief description of the experimental arrangement and method. The subsequent section contains the presentation and discussion of the experimental results and is organized in four subsections. The first subsection presents the branching ratio of all product channels as a function of collision energy, whereas the three next subsections show a detailed analysis of each product channel in terms of angle- and energy differential cross sections. The results for the proton transfer reaction channel are additionally compared with the results for $OH^- + CH_3I$[35,36] and with recent theoretical predictions for the dynamics of proton transfer in $F^- + CH_3I$.[37]

■ EXPERIMENTAL METHOD

Our experimental setup to study ion−molecule reactive scattering combines a crossed beam arrangement with a velocity map imaging spectrometer. Compared to our previously reported measurements on the $F^- + CH_3I$ reaction,[33] the setup has been considerably improved. A detailed description of the new features has been given in recent publications.[12,38]

The reactant ions are produced by dissociative electron attachment to NF_3 in a mixture of approximately 10% NF_3 in argon in a pulsed plasma discharge source. The generated F^- ions are subsequently accelerated toward an octupole radio-frequency ion trap using a Wiley−McLaren time-of-flight spectrometer. In the trap, the F^- ions are stored for tens of milliseconds, whereby the ion cloud is cooled with respect to its position and energy spread in a helium buffer gas. After being accelerated out of the trap again, the ions are decelerated to the selected kinetic energy and crossed with a supersonic neutral beam (<3% CH_3I in helium) at a relative collision angle of 60° in the interaction region of a differentially pumped scattering chamber.

After the reactants have crossed, the field plates of the velocity map imaging (VMI) spectrometer are activated, and if created, a product ion is extracted perpendicular to the scattering plane onto a time- and position-sensitive detector, consisting of a microchannel plate (MCP), a phosphor screen, and a photomultiplier. The impact position of each reactive event is recorded by a charge-coupled device (CCD) camera and transformed into a velocity vector in the plane of the detector. The photomultiplier records the arrival time information on each product ion, which is used to identify the product ion mass and to determine its velocity component perpendicular to the detector plane. In total, we thus obtain a three-dimensional velocity image in the center of mass frame, which represents the differential scattering cross section. The entire experiment is operated at a repetition rate of 20 Hz.

Reactive scattering is conducted at several collision energies by adjusting the ions' translational energy, whose distribution is described by a full-width at half-maximum (fwhm) in the range of 160−250 meV. The pulsed valve generating the neutral beam is heated in order to avoid CH_3I condensation in the nozzle. The velocity and translational temperature of the neutral reactants is obtained by electron impact ionization of the supersonic beam and subsequent imaging of the produced CH_3I^+ ions. We obtain an average neutral beam velocity of 1300 m/s. For the translational temperature, an upper limit of 150 K is estimated, limited by the broadening of the velocity spread due to the momentum transfer from the impinging high energy electrons. The concentration and backing pressure of the neutral reactants are optimized to <3% and <0.7 bar in order to avoid possible clustering of the neutral reactant.

■ RESULTS AND DISCUSSION

Branching Ratios. We have performed a reactive scattering experiment between fluorine anions and methyl iodide at eight different collision energies, ranging from 0.4 to 0.9 eV. The resulting product ion branching ratio as a function of collision energy is presented in Figure 1, together with an illustrative time-of-flight spectrum of the product ions. The spectrum shows the four products formed during the reaction, I^- (m/z = 127), CH_2I^- (m/z = 141), IF^- (m/z = 146), and $[FHI]^-$ (m/z = 147). The calculated reaction enthalpies for the formation of these products can be extracted from Table 1.

The dominating product at all energies is I^-. This anion is essentially produced via the classical nucleophilic substitution reaction, a process that is exothermic by 1.84 eV. This pathway
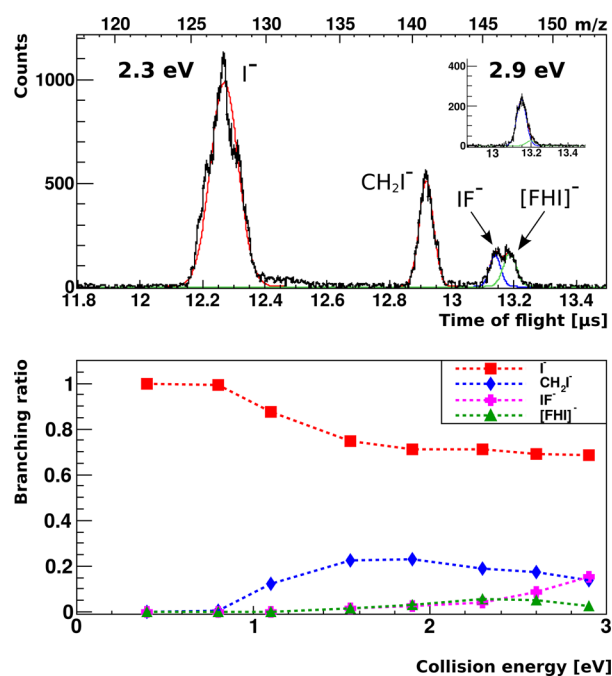
Figure 1. Time-of-flight spectrum and branching ratio of the product masses formed in F⁻ + CH₃I reactive scattering. Top: exemplary time-of-flight mass spectrum for the F⁻ + CH₃I reaction at 2.3 eV collision energy. The four observed masses stem from a nucleophilic displacement reaction forming I⁻, a proton transfer reaction that leads to CH_2I^- products, a halogen abstraction mechanism forming IF⁻, and a hydrogen–dihalide complex, [FHI]⁻. The red solid line represents a fit to all product peaks. The upper x-axis depicts the corresponding mass-to-charge ratio. The blue and green solid lines illustrate the individual contributions of the two dihalide species. The inset shows the dihalide anions at the highest studied collision energy of 2.9 eV. Bottom: branching ratio of the different product channels as a function of collision energy. The contribution of each product is determined by Gaussian fitting the area under each time-of-flight distribution. Statistical errors were determined for each point; however, in all cases, these error bars are hidden by the markers.

Table 1. Standard Enthalpies of Reaction for the Different Products in F⁻ + CH₃I Calculated from Enthalpies of Formation at 0 K

products	$\Delta_r H°$ [eV]
F⁻ + CH₃I	0
I⁻ + CH₃F	−1.84[a]
CH_2I^- + HF	0.6 ± 0.1[b]
	0.73[c]
IF⁻ + CH₃	0.7 ± 0.3[d]
FHI⁻ + CH₂	0.9 ± 0.2[e]

[a]Calculated using tabulated electron affinities and gas phase standard formation enthalpies.[40] [b]Calculated using the tabular reaction enthalpies for CH₃I → CH_2I^- + H⁺ and H⁺ + F⁻ → HF.[40] [c]Taken from ref 37. [d]Calculated using the electron affinity of iodine[40] and an electron affinity of IF of 2.5 eV [e]Calculated taking the reaction enthalpies for HF + I⁻ → FH-I⁻ from ref 41, the electron affinities of iodine and fluorine,[40] and the tabulated gas phase standard enthalpies of formation for CH₃I, HF and CH₂.[41]

exhibits a very small central potential energy barrier, a fact attributed to the strong nucleophilicity of fluorine and the strong C−F bond in the product CH₃F.[34,39] The angle- and energy differential cross sections for this channel have already been investigated.[33] The branching ratio for this channel is

maximal at low energies. It decreases to below 0.7 with the opening of the three other channels, on which we will focus in the following, but it remains the dominant channel.

As can be seen in Table 1, the three alternative channels are energetically endothermic. While their tabulated endoergicities are similar, their observed threshold behavior, specifically their appearance energies, is markedly different (see Figure 1). The proton transfer product, CH_2I^-, starts to be formed already at an energy that corresponds to its reaction enthalpy, at about E_{col} = 0.8 eV. This is in agreement with a very recent electronic structure calculation on the proton transfer channel for this system, which predicts no transition state barrier above the product CH_2I^- + HF energy.[37] At increasing collision energy, its branching ratio strongly increases, reaching a maximum branching ratio of 0.2 at 1.9 eV. At higher energies, the branching ratio starts to decrease, possibly associated with the opening of other reaction products as for example the 1.9 eV endothermic I⁻ + CH₂ + HF formation. In contrast to the proton transfer channel, dihalide production (IF⁻) is only detected at energies substantially above its reaction enthalpy. While not directly implied, this could be an indication of an effective barrier higher than its reaction enthalpy.

Moreover, the branching ratio of IF⁻ starts to rise only very slowly with increasing collision energy. This implies a steeper rising cross section for the proton transfer channel. Between 2.3 and 2.9 eV a strong increase is observed for the IF⁻ product branching ratio. This hints toward a second threshold, possibly related to surmounting the C−I bond strength at relative collision energies exceeding 2.6 eV. A very similar behavior was observed for two related systems (F⁻ + CH₃Cl and Cl⁻ + CH₃Br) in detailed measurements of their absolute reaction cross sections.[22,28] In these publications, the authors postulate a collision-induced rupture of the C−I bond accompanied by dihalide bond formation in order to explain the sharp increase of IF⁻ at increased collision energies.

In addition to the discussed product channels, a fourth mass corresponding to a stable [FHI]⁻ anion complex is observed starting from 1.55 eV. This product has not been reported to date in previous (S$_N$2) studies, even though it has been found to be an energetically stable species in a recent theoretical work.[42] In that publication, a possible [FH − I]⁻ structure of this complex is discussed. However, as the formation mechanism and thus the structure of this anion is not evident in our experiments, we will write the complex structure in brackets, [FHI]⁻, throughout this publication. In principle, the ion could be formed via a dihalide intermediate attacking an H atom or via an F−H bounded complex binding to the halogen before dissociation. Due to the low reactant densities in our scattering region, we can safely neglect secondary reactions between free reaction products (e.g., HF + I⁻).

The branching ratio of this product mass evolves with energy in a very similar way to the dihalide formation channel, as can be seen in the lower graph of Figure 1. After reaching a maximum branching ratio of around 0.07, its intensity decreases again at high energies, which could be an indication for a dissociation threshold. Although no potential energy landscape exists that shows possible crossings with other dissociative channels at energies of around 2.9 eV, it appears to be plausible that the hydrogen-dihalide anion decays again into HF and I⁻ if it is internally excited. The first observation of this hydrogenated dihalide product ion, together with the fact that it only appears in a narrow energy range, will hopefully stimulate theoretical calculations for this intriguing pathway.
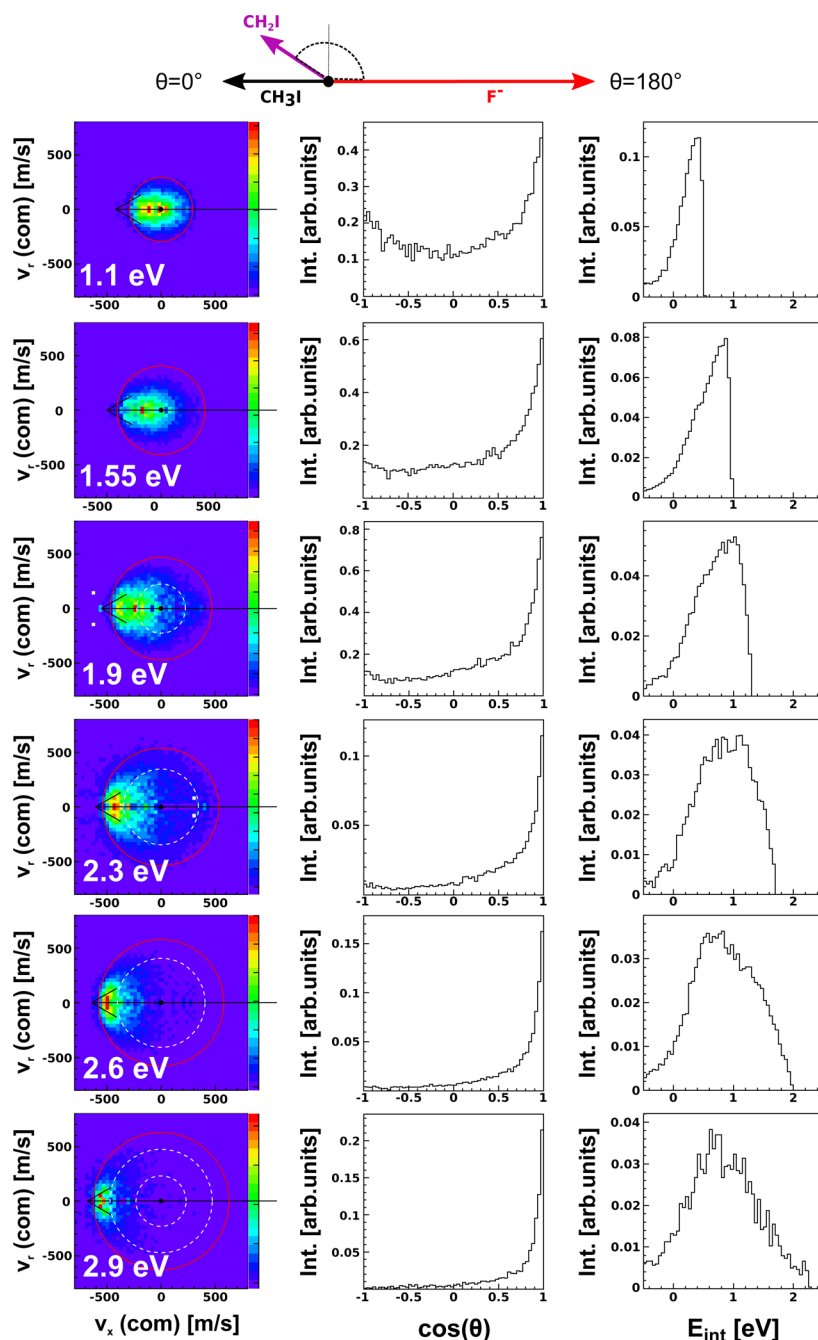
Figure 2. Experimental reactive scattering results for the reaction of F⁻ + CH₃I → HF + CH₂I⁻. Left column: 3D velocity distributions, mapped onto 2D histograms, of the product CH₂I⁻ ion in the center of mass frame for a series of increasing collision energies. Central column: velocity-integrated angular distributions for the product CH₂I⁻ ion as a function of collision energy, illustrating the evolution toward strongly dominant forward scattering. Right column: internal energy distributions of the reaction products. The y-axes of all scattering angle and internal energy histograms represent normalized counts.

In order to gain a deeper understanding on the dynamical and kinematical properties of all three observed product ion channels, the next subsections present experimental angle- and energy differential cross sections for each product as a function of collision energy.

CH₂I⁻ Channel. The angle- and energy differential results from reactive scattering for the proton transfer product CH₂I⁻ are depicted in Figure 2. Due to the very low signal intensity at 0.8 eV relative collision energy, we do not analyze the scattering features at this energy. The left column of Figure 2 shows the longitudinal and transverse velocity distributions of product

CH₂I⁻ ions in the center of mass frame, mapped onto a two-dimensional image.

The images illustrate the dynamical and kinematical evolution of the reaction as a function of collision energy. The depicted red solid circle represents the kinematic limits for the reaction, $E_{\text{limit}} = (E_{\text{col}} + \Delta_r H^\circ)$, whereas the white dashed circles represent 1 eV spaced spheres. The relevant velocity vectors for the reaction are depicted in the Newton diagram above the images. Although the reaction enthalpy given in ref.[37] was determined in an accurate calculation, the value of 0.6 eV was chosen in this work for $\Delta_r H^\circ$, in order to be consistent

with the other values also obtained from tabulated formation enthalpies (see Table 1). In order to further analyze the features of the images, the central column depicts the distribution of the velocity-integrated scattering angle of the product ion, whereas the panels of the right column show the internal energy distribution, that is the amount of initially available energy transferred into product internal degrees of freedom.

At low collision energies, we observe products scattered into all possible directions with a velocity distribution peaking at zero in the center of mass frame. In previous studies on the nucleophilic substitution channel, this velocity distribution was ascribed to a transition state complex with a lifetime longer than its rotational period.[16] This analogy may suggest a similar mechanism for the proton transfer pathway at these collision energies. As the collision energy increases, the product velocity distribution becomes centered along the CH_3I velocity vector, close to the kinematical cutoff. Such a direct mechanism with low momentum transfer to the CH_3I reactant is defined as forward scattering and its directionality contrasts with the rather isotropic distribution at low energies. While at intermediate energies both mechanisms seem to compete, the direct forward scattering completely dominates the dynamics at the two highest energies, as can be extracted from the very asymmetric scattering angle distributions of Figure 2.

Regarding the internal energy distribution in the right column, a decrease of the fraction of energy transferred into product internal excitation can be observed for the four highest collision energies. The mean internal energy peaks at around 1 eV for 1.9 and 2.3 eV collision energy, whereas it decreases to 0.6−0.7 eV for the two highest collision energies. In particular, the transition is very obvious between 2.3 and 2.6 eV collision energy (see next subsection for quantitative details).

Comparison with OH^- + CH_3I Reaction and F^- + CH_3I Trajectory Calculation. In their recent study, Hase and co-workers have theoretically investigated the proton transfer reaction in F^- + CH_3I.[37] In this work, both electronic structure calculations at the DFT/B97−1/aug-cc-pVDZ level of theory and direct dynamics simulations at the single relative collision energy of 1.55 eV have been performed. The obtained potential energy surface predicts two mechanistic paths through several transition states toward the endothermic product formation, both of which include an I-HF bonded postreaction complex.

As OH^- is isoelectronic to F^- and also has a very high proton affinity, it is of great interest to compare the proton transfer dynamics of both nucleophiles with CH_3I. Two recent experimental and theoretical studies on the OH^- + CH_3I reaction have evaluated the proton transfer channel leading to H_2O + CH_2I^-.[35,36] A detailed analysis of the internal energy excitation was presented and the energy partitioning into vibrational and rotational modes was computed. A hydrogen-bonded complex was found to be the energetically stable entrance channel geometry. In addition, an investigation of the branching ratio between the different channels showed clear formation of reaction products of type (2) and (3). In particular, proton transfer is strongly competing with nucleophilic substitution at all relative energies in that system.

Electronic structure calculations have confirmed the presence of a stable hydrogen-bonded ion−dipole prereaction complex for both F^- + CH_3I and OH^- + CH_3I,[30] which might contribute to the high cross section for proton transfer observed in both cases. The main difference arises from the slight exothermic character of the proton transfer reaction for

OH^- + CH_3I in contrast to the endothermic character of proton transfer in F^- + CH_3I. For the latter, the H-bonded prereaction complex is the only point of the potential surface energetically submerged with respect to the reactant asymptote. In fact, both prereaction complexes show not only the same H-bonded geometry but also an equivalent energy of −0.87 eV with respect to the reactants. Given these energetic similarities, it becomes interesting to evaluate if the dynamics and kinematics of both reactions differ significantly from each other.

In Table 2, we present our experimental average internal energy fraction as a function of collision energy and compare

Table 2. Average Experimental and Simulated Fraction of Energy Partitioned into Product Internal Excitation as a Function of Relative Collision Energy[a]

	E_{rel} [eV]	f_{int} (exp)	f_{int} (sim)
F^- + $CH_3I \rightarrow HF$ + CH_2I^-	1.1	0.41 ± 0.08	-
	1.55	0.56 ± 0.10	0.39 ± 0.07
		0.48 ± 0.10[b]	
	1.9	0.51 ± 0.10	-
	2.3	0.47 ± 0.11	-
	2.6	0.41 ± 0.12	-
	2.9	0.35 ± 0.13	-
OH^- + $CH_3I \rightarrow H_2O$ + CH_2I^-	0.5	0.48 ± 0.14	0.51 ± 0.04
	1.0	0.53 ± 0.09	0.46 ± 0.02
	1.5	0.44 ± 0.05	-
	2.0	0.40 ± 0.04	0.29 ± 0.03

[a]The data for the OH^- + CH_3I reaction stems from ref 36. The experimental errors for both systems were obtained by convoluting the collision energy uncertainties with the root mean square of the respective mean internal energy. The theoretical value for F^- + CH_3I at 1.55 eV is taken from ref 37. [b]Obtained using the exothermicity value given in ref 37 (see text for details).

these results with the computational and experimental fractions for the related system of ref 36. For the collision energy of 1.55 eV, the fraction is also compared with the theoretical result of ref 37. Not listed in this table is the specific energy partitioning for product rotational and vibrational energies obtained in the trajectory calculations performed for each system. For both reactions, the specific partitioning shows that the energy is mainly transferred to vibrational and rotational modes of CH_2I^-, whereas the neutral product appears mainly in the vibrational ground state.[35,37]

The simulated internal energy fraction for 1.55 eV collision energy amounts to 0.39 ± 0.07. It lies below the experimental value with a difference that is slightly larger than the estimated accuracies. The experimental data has been analyzed using the exothermicity of 0.6 eV for this channel to be consistent with the other product channels (as discussed above). If the value of 0.73 eV, calculated in ref 37 (see Table 1), is employed instead, the experimental internal energy fractions decreases and becomes 0.48 ± 0.10 at 1.55 eV (see Table 2). This value agrees within the error bars with the simulation.

The simulations find that the proton transfer channel proceeds via backward, forward and indirect scattering dynamics, with forward and isotropic scattering possessing the largest cross sections. This is in agreement with the experimental findings, which show that the combination of these latter mechanisms dominates at 1.55 eV.

Our present results show a very considerable amount of initially available energy being partitioned to product excitation.
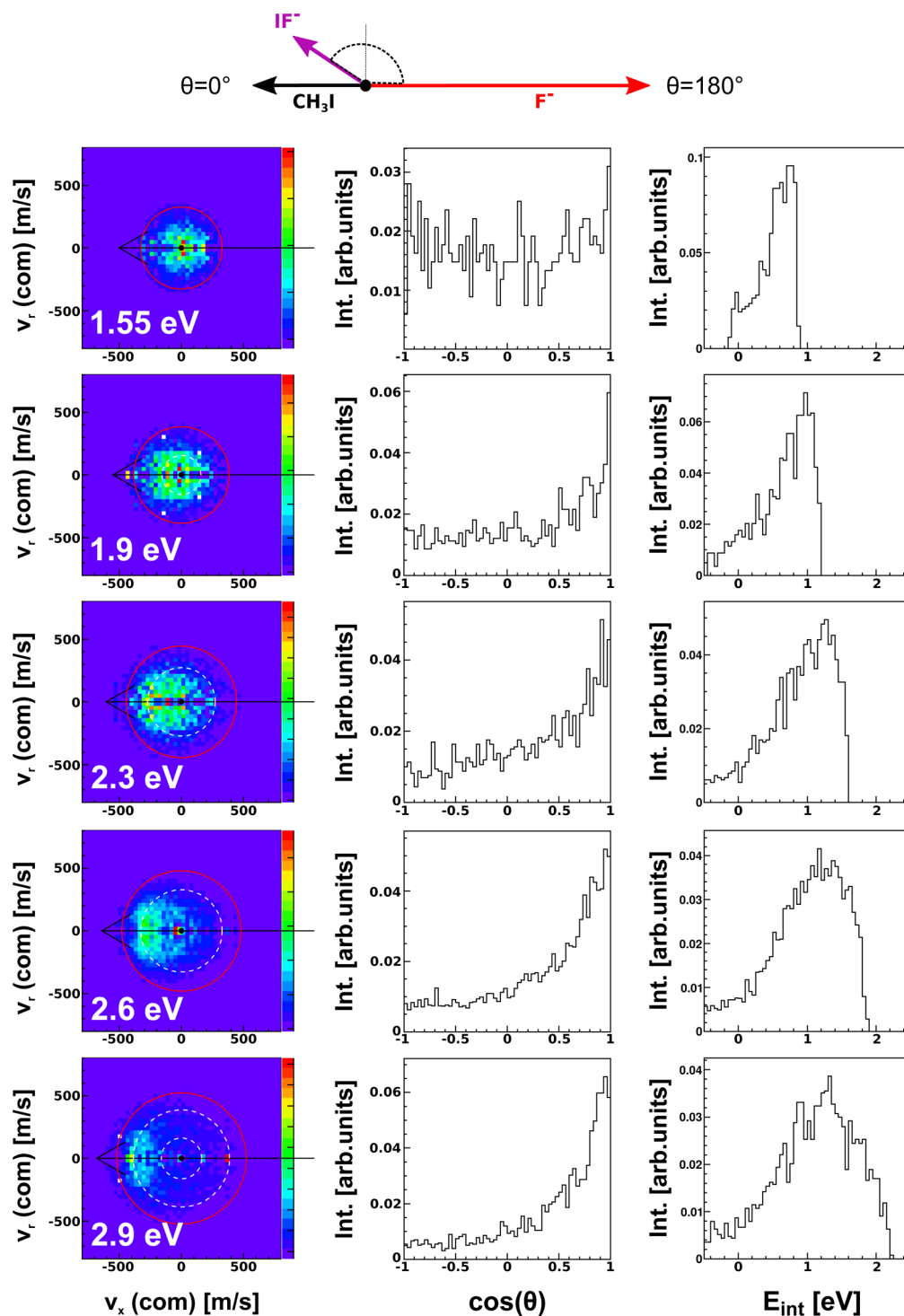
Figure 3. Experimental reactive scattering results for the reaction of $F^- + CH_3I \rightarrow CH_3 + IF^-$. The three columns describe the data in the same manner as in Figure 2. Due to the low signal intensity at 1.1 eV, a detailed analysis has only been performed for the five higher relative collision energies.

At 1.1 eV, the fraction amounts to 0.4, further increasing to 0.56 of the initially available energy. At the two highest energies, however, the excited fraction is decreased again to 0.35. The proton transfer channel for $OH^- + CH_3I$ shows similar absolute values for the internal energy fraction, ranging from 0.4 to 0.53 and an equivalent collision energy dependent relative internal excitation. The energy transfer into translational motion becomes efficient at a higher energy for $F^- +$ CH_3I. For the highest energies, no direct comparison is possible as no data above 2.0 eV was taken for $OH^- + CH_3I$.

The similarities in the behavior contrast with the abovementioned differences in the potential energy surfaces of both reactions.[30,32,37] However, both minimum energy paths possess an equivalent prereaction complex, regarding both structure and energetics. The similar trends described here could indicate that it is essentially the shape of the entrance-channel that
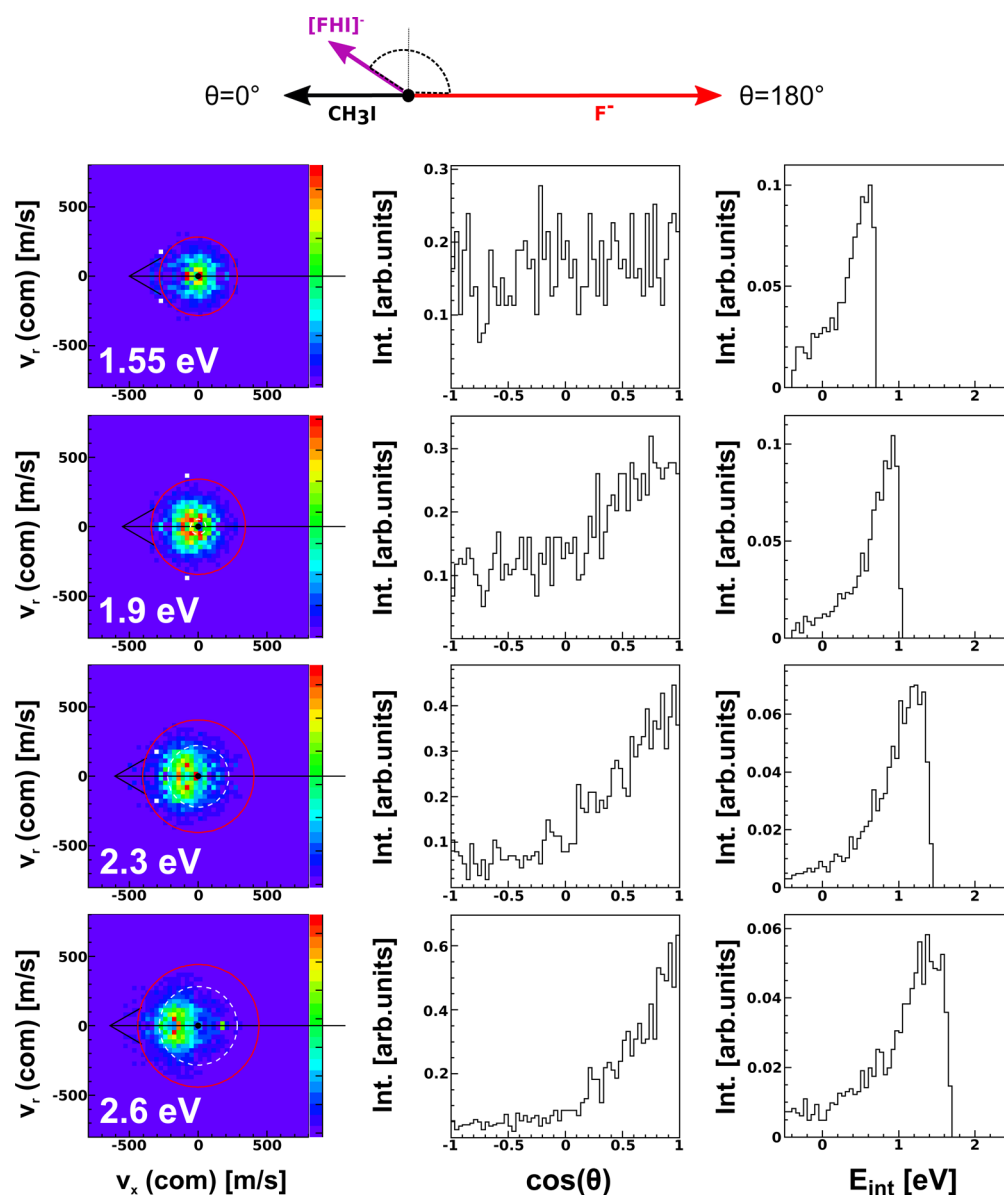
Figure 4. Experimental reactive scattering results for the reaction of $F^- + CH_3I \rightarrow CH_3 + FHI^-$. The three columns describe the data in the same way as in Figures 2 and 3

influences the dynamics and kinematics of these proton transfer reactions.

IF$^-$ Channel. The results for the endothermic halogen abstraction product IF$^-$ are depicted in Figure 3. The figure is organized in the same manner as in the proton transfer case, presenting experimental results at five collision energies. As can be observed in the upper panel of Figure 1, the overlap of the IF$^-$ and FHI$^-$ time-of-flight distributions may lead to a partial contamination in the velocity images due to wrong event assignment, especially at the highest collision energies. In order to clearly separate the images of the two closely lying species, narrow time-of-flight cuts were therefore chosen such that only a minimal fraction of adjacent events may potentially contaminate the respective velocity images.

The dihalide formation reaction shows a qualitatively similar behavior as the proton transfer mechanism. As can be inferred by looking at the velocity distributions in the left column and is confirmed by the depicted scattering angle distributions, the exit of the product ion evolves from an isotropic scattering at

the lowest analyzed relative collision energy of 1.55 eV toward a dominant forward scattering process.

To our knowledge, no trajectory calculations have been carried out on this specific reaction. However, the mechanism could occur through the formation of a collision complex via halophilic attack at the iodine. In a recent investigation we have presented the strong attractive I–F interaction in the CH$_3$I···F$^-$ complex in contrast to the much weaker Cl–F interaction.[18] In that publication, we discuss that this attraction may stabilize the F–I bonded prereaction complex and how this may hinder the orientation toward the collinear backward structure in F$^-$ + CH$_3$I and thereby facilitate the observed indirect dynamics at high relative collision energies.[33] In addition, it may explain the considerable branching ratio observed here for IF$^-$ as compared to the reaction with OH$^-$.[35]

For the dihalide formation channel a considerable amount of energy is partitioned into internal excitation, as shown in the right panels of Figure 3. In contrast to the proton transfer channel, the mean internal energy peaks at around 1.0−1.2 eV

for a collision energy of 1.9 eV and exhibits almost no dependence on increasing collision energy. This may indicate that the same internal modes are being excited throughout the higher energy range. Compared to the CH_2I^- proton transfer channel, the observed excitation of the products' internal degrees of freedom is significantly larger for IF^- formation.

[FHI]⁻ Channel. As described above, we have found evidence for a third reaction competing with nucleophilic substitution, namely, the one forming the hydrogenated dihalide anion $[FHI]^-$. Its contribution is as strong as the bare dihalide for energies ranging from 1.55−2.3 eV (see Figure 1). In Figure 4, we show the analyzed experimental results for this fourth channel in $F^- + CH_3I$ as a function of collision energy. As explained before, it cannot be excluded that a minimal fraction of the presented product events corresponds to wrongly assigned IF^-. This is particularly important at 2.9 eV relative collision energy, where the strong increase of IF^- product branching relative to $[FHI]^-$ causes a substantial time-of-flight overlap between both species. Therefore, this collision energy has not been analyzed for the $[FHI]^-$ product.

The velocity distributions for $[FHI]^-$ show similar features as for IF^-, with an isotropic velocity distribution at low energies and an increasing forward scattering fraction at high energies. The relative amount of energy partitioned into product excitation is higher for this anion than for IF^- and may be an indication of a long-lived complex preceding dissociation. This high internal excitation may also promote the dissociation of the hydrogen-dihalide ion at high energies, which could explain the decrease of its branching ratio observed in Figure 1.

To our knowledge, there is no previous report on the formation of this hydrogen−dihalide complex for similar systems, a fact that makes it challenging to ascribe specific dynamical features to the observed velocity- and scattering angle distributions. In principle, two possible prereaction complexes are plausible, namely, $FH–I^-$ and $H–FI^-$. The first case would correlate with the formation of the stable H-bonded complex followed by a halogen capture during the complex lifetime. In the second case, F^- would bind to the iodine producing a complex of C_{3v} symmetry, followed by a hydrogen-bond formation. Potential energy calculations only have been reported for the first possible complex.[42]

As mentioned in the section devoted to the proton transfer mechanism, a recent calculation on this pathway predicts the existence of a stable $[CH_2I^- –HF]$ postreaction complex geometry.[37] This complex is formed through migration of HF from the carbon to the iodine atom, either clockwise or counterclockwise. Although this work does not mention an alternative product formation, the structure of the postreaction complex may hint toward the formation of an $FH–I^-$ ion.

These structural considerations, together with the fact that nonstandard dynamics have already been observed for similar systems,[19,21] may stimulate trajectory calculations to be performed on this intriguing product channel. This would be very helpful in order to understand the geometry of both entrance and exit channel complexes, as well as possible crossings with dissociation channels that may explain the small energy range where this species is observed.

CONCLUSIONS

Branching ratios and angle- and energy differential cross sections have been obtained for three endothermic reactions competing with nucleophilic substitution in $F^- + CH_3I$ as a function of relative collision energy (0.4−2.9 eV) using a crossed beam arrangement in combination with three-dimensional velocity map imaging detection. Detected product ions are CH_2I^-, IF^-, and $[FHI]^-$. The first two ions are known to be produced via proton transfer and halogen abstraction, respectively.[28,36] The latter species, which has not been observed in similar systems to date, may occur through an H-bonded prereaction complex, followed by HF migration to the iodine atom and subsequent rupture of the C−I bond.

The S_N2 channel dominates the product branching at all investigated collision energies. Its relative abundance decreases with increasing collision energies. The proton transfer experiences a sudden rise at 1.1 eV and reaches a maximal branching ratio of about 0.2 before decreasing in intensity beyond 2.3 eV. Both IF^- and $[FHI]^-$ appear at 1.55 eV and show a small contribution until 2.6 eV, where $[FHI]^-$ decreases while IF^- experiences a stronger second increase and becomes the second most dominant product.

The velocity distributions of all three products show similar trends, with isotropic scattering and direct forward scattering dominating at low and high relative energies, respectively. Regarding the internal energy distributions, the absolute energy transferred into product internal degrees of freedom is found to be relatively independent of collision energy for IF^- and $[FHI]^-$, whereas it decreases at higher energies for the proton transfer product CH_2I^-. For this latter pathway, a comparison with the isoelectronic $OH^- + CH_3I$ reaction shows a similar trend of the internal energy fraction for increasing collision energies. Moreover, our experiments show a slightly higher fraction of internal excitation at $E_{col} = 1.55$ eV than predicted in recent theoretical work,[37] albeit compatible within the experimental accuracy.

This experimental investigation sheds more light onto the variety of alternative reactions to the classical nucleophilic substitution at higher collision energies and presents new dynamical and kinematical insights that will hopefully stimulate further trajectory calculations on these pathways. In particular, the appearance of the $[FHI]^-$ ion opens up new questions about the complex mechanistic behavior along the reaction coordinate and may be an interesting subject for future theoretical investigations.

AUTHOR INFORMATION

Corresponding Author

*E-mail: roland.wester@uibk.ac.at. Phone: +43 512 507 52620.

Notes

The authors declare no competing financial interest.

REFERENCES

(1) Walden, P. Über die Gegenseitige Umwandlung Optischer Antipoden. *Ber. Dtsch. Chem. Ges.* **1896**, *29*, 133−138.

(2) Hughes, E. D.; Ingold, C. K. Mechanism of Substitution at a Saturated Carbon atom. Part IV. A Discussion of Constitutional and Solvent Effects on the Mechanism, Kinetics, Velocity and Orientation of Substitution. *J. Chem. Soc.* **1935**, 244−255.

(3) Olmstead, W.; Brauman, J. Gas-Phase Nucleophilic Displacement Reactions. *J. Am. Chem. Soc.* **1977**, *99*, 4219.

(4) Barlow, S. E.; Doren, J. M. V.; Bierbaum, V. M. The Gas Phase Displacement Reaction of Chloride Ion with Methyl Chloride as a Function of Kinetic Energy. *J. Am. Chem. Soc.* **1988**, *110*, 7240−7242.

(5) Viggiano, A. A.; Morris, R. A.; Paschkewitz, J. S.; Paulson, J. F. Kinetics of the Gas-Phase Reactions of Chloride Anion, Cl⁻ with CH₃Br and CD₃Br: Experimental Evidence for Nonstatistical Behavior? *J. Am. Chem. Soc.* **1992**, *114*, 10477−10482.

(6) Hase, W. L. Simulations of Gas-Phase Chemical Reactions: Applications to S_N2 Nucleophilic Substitution. *Science* **1994**, *266*, 998−1002.

(7) Wang, H.; Hase, W. L. Kinetics of F⁻ + CH₃Cl S_N2 Nucleophilic Substitution. *J. Am. Chem. Soc.* **1997**, *119*, 3093−3102.

(8) Vayner, G.; Houk, K. N.; Jorgensen, W. L.; Brauman, J. I. Steric Retardation of S_N2 Reactions in the Gas Phase and Solution. *J. Am. Chem. Soc.* **2004**, *126*, 9054−9058.

(9) Uggerud, E. Reactivity Trends and Stereospecificity in Nucleophilic Substitution Reactions. *J. Phys. Org. Chem.* **2006**, *19*, 461−466.

(10) Chabinyc, M. L.; Craig, S. L.; Regan, C. K.; Brauman, J. I. Gas-Phase Ionic Reactions: Dynamics and Mechanism of Nucleophilic Displacements. *Science* **1998**, *279*, 1882−1886.

(11) Bierbaum, V. M. Go with the Flow: Fifty Years of Innovation and Ion Chemistry Using the Flowing Afterglow. *Int. J. Mass Spectrom.* **2015**, *377*, 456−466. Special Issue: {MS} 1960 to Now.

(12) Trippel, S.; Stei, M.; Otto, R.; Hlavenka, P.; Mikosch, J.; Eichhorn, C.; Lourderaj, U.; Zhang, J. X.; Hase, W. L.; Weidemüller, M.; et al. Kinematically Complete Chemical Re-action Dynamics. *J. Phys. Conf. Series* **2009**, *194*, 012046.

(13) Sun, L.; Song, K.; Hase, W. L. A S_N2 Reaction That Avoids Its Deep Potential Energy Minimum. *Science* **2002**, *296*, 875−878.

(14) Bento, A. P.; Bickelhaupt, F. M. Nucleophilicity and Leaving-Group Ability in Frontside and Backside S_N2 Reactions. *J. Org. Chem.* **2008**, *73*, 7290−7299.

(15) Szabo, I.; Csaszar, A. G.; Czako, G. Dynamics of the F⁻ + CH₃Cl → Cl⁻ + CH₃F S_N2 Reaction on a Chemically Accurate Potential Energy Surface. *Chem. Sci.* **2013**, *4*, 4362−4370.

(16) Xie, J.; Otto, R.; Mikosch, J.; Zhang, J.; Wester, R.; Hase, W. L. Identification of Atomic-Level Mechanisms for Gas-Phase X⁻ + CH₃Y S_N2 Reactions by Combined Experiments and Simulations. *Acc. Chem. Res.* **2014**, *47*, 2960.

(17) Otto, R.; Brox, J.; Trippel, S.; Stei, M.; Best, T.; Wester, R. Single Solvent Molecules can Affect the Dynamics of Substitution Reactions. *Nat. Chem.* **2012**, *4*, 534−538.

(18) Stei, M.; Carrascosa, E.; Kainz, M. A.; Kelkar, A.; Meyer, J.; Szabo, I.; Czako, G.; Wester, R. Influence of the Leaving Group on the Dynamics of a Gas Phase S_N2 Reaction. *Nat. Chem.* **2016**, *8*, 151−156.

(19) Mikosch, J.; Trippel, S.; Eichhorn, C.; Otto, R.; Lourderaj, U.; Zhang, J.; Hase, W.; Weidemüller, M.; Wester, R. Imaging Nucleophilic Substitution Dynamics. *Science* **2008**, *319*, 183.

(20) Manikandan, P.; Zhang, J.; Hase, W. L. Chemical Dynamics Simulations of X⁻ + CH₃Y → XCH₃ + Y⁻ Gas-Phase S_N2 Nucleophilic Substitution Reactions. Nonstatistical Dynamics and Nontraditional Reaction Mechanisms. *J. Phys. Chem. A* **2012**, *116*, 3061−3080.

(21) Szabo, I.; Czako, G. Double-Inversion Mechanisms of the X⁻ + CH₃Y [X,Y = F, Cl, Br, I] S_N2 Reactions. *J. Phys. Chem. A* **2015**, *119*, 3134−3140.

(22) Angel, L. A.; Ervin, K. M. Dynamics of the Gas-Phase Reactions of Fluoride Ions with Chloromethane. *J. Phys. Chem. A* **2001**, *105*, 4042−4051.

(23) Yang, Z.-Z.; Ding, Y.-L.; Zhao, D.-X. Theoretical Analysis of Gas-Phase Front-Side Attack Identity S_N2(C) and S_N2(Si) Reactions with Retention of Configuration. *J. Phys. Chem. A* **2009**, *113*, 5432−5445.

(24) Zhang, J.; Mikosch, J.; Trippel, S.; Otto, R.; Weidemüller, M.; Wester, R.; Hase, W. L. F⁻ + CH₃I → FCH₃ + I⁻ Reaction Dynamics. Nontraditional Atomistic Mechanisms and Formation of a Hydrogen-Bonded Complex. *J. Phys. Chem. Lett.* **2010**, *1*, 2747−2752.

(25) Szabo, I.; Telekes, H.; Czako, G. Accurate ab Initio Potential Energy Surface, Thermochemistry, and Dynamics of the F⁻ + CH₃F

S_N2 and Proton-Abstraction Reactions. *J. Chem. Phys.* **2015**, *142*, 244301.

(26) Hierl, P.; Henchman, M.; Paulson, J. Threshold Energies for the Reactions OH⁻ + CH₃X → CH₃OH + X⁻ (X = Cl, Br) Measured by Tandem Mass Spectrometry: Deprotonation Energies (Acidities) of CH₃Cl and CH₃Br. *Int. J. Mass Spectrom. Ion Processes* **1992**, *117*, 475−485.

(27) Wilbur, J. L.; Wladkowski, B. D.; Brauman, J. I. Gas-phase Proton-Transfer and Substitution Reactions: Energy Dependence and Dissociation Dynamics. *J. Am. Chem. Soc.* **1993**, *115*, 10823−10829.

(28) Angel, L. A.; Ervin, K. M. Gas-Phase S_N2 and Bromine Abstraction Reactions of Chloride Ion with Bromomethane: Reaction Cross Sections and Energy Disposal into Products. *J. Am. Chem. Soc.* **2003**, *125*, 1014−1027.

(29) Angel, L. A.; Ervin, K. M. Gas-Phase Reactions of the Iodide Ion with Chloromethane and Bromomethane: Competition between Nucleophilic Displacement and Halogen Abstraction. *J. Phys. Chem. A* **2004**, *108*, 9827−9833.

(30) Xie, J.; Zhang, J.; Hase, W. L. Is There Hydrogen Bonding for Gas Phase S_N2 pre-reaction Complexes? *Int. J. Mass Spectrom.* **2015**, *378*, 14−19.

(31) Cyr, D. M.; Scarton, M. G.; Wiberg, K. B.; Johnson, M. A.; Nonose, S.; Hirokawa, J.; Tanaka, H.; Kondow, T.; Morris, R. A. Observation of the XY⁻ Abstraction Products in the Ion−Molecule Reactions X⁻ + RY → XY⁻ + R: An Alternative to the S_N2 Mechanism at Suprathermal Collision Energies. *J. Am. Chem. Soc.* **1995**, *117*, 1828−1832.

(32) Sun, R.; Xie, J.; Zhang, J.; Hase, W. L. The F⁻ + CH₃I → FCH₃ + I⁻ Entrance Channel Potential Energy Surface: Comparison of Electronic Structure Methods. *Int. J. Mass Spectrom.* **2015**, *377*, 222−227. Special Issue: {MS} 1960 to Now.

(33) Mikosch, J.; Zhang, J.; Trippel, S.; Eichhorn, C.; Otto, R.; Sun, X.; de Jong, W.; Weidemüller, M.; Hase, W.; Wester, R. Indirect Dynamics in a Highly Exoergic Substitution Reaction. *J. Am. Chem. Soc.* **2013**, *135*, 4250.

(34) Sun, R.; Davda, C. J.; Zhang, J.; Hase, W. L. Comparison of Direct Dynamics Simulations with Different Electronic Structure Methods. F⁻ + CH₃I with MP2 and DFT/B97−1. *Phys. Chem. Chem. Phys.* **2015**, *17*, 2589−2597.

(35) Otto, R.; Xie, J.; Brox, J.; Trippel, S.; Stei, M.; Best, T.; Siebert, M. R.; Hase, W. L.; Wester, R. Reaction Dynamics of Temperature-Variable Anion Water Clusters Studied with Crossed Beams and by Direct Dynamics. *Faraday Discuss.* **2012**, *157*, 41−57.

(36) Xie, J.; Sun, R.; Siebert, M. R.; Otto, R.; Wester, R.; Hase, W. L. Direct Dynamics Simulations of the Product Channels and Atomistic Mechanisms for the OH⁻ + CH₃I Reaction. Comparison with Experiment. *J. Phys. Chem. A* **2013**, *117*, 7162−7178.

(37) Zhang, J.; Xie, J.; Hase, W. L. Dynamics of the F⁻ + CH₃I → HF + CH₂I⁻ Proton Transfer Reaction. *J. Phys. Chem. A* **2015**, *119*, 12517−12525.

(38) Wester, R. Velocity Map Imaging of Ion−Molecule Reactions. *Phys. Chem. Chem. Phys.* **2014**, *16*, 396−405.

(39) Glukhovtsev, M. N.; Pross, A.; Radom, L. Gas-Phase Non-Identity S_N2 Reactions of Halide Anions with Methyl Halides: A High-Level Computational Study. *J. Am. Chem. Soc.* **1996**, *118*, 6273−6284.

(40) NIST. *NIST Chemistry WebBook, NIST Standard Reference Database Number 69*; National Institute of Standards and Technology: Gaithersburg MD, 2015.

(41) Lide, D. R. *CRC Handbook of Chemistry and Physics*, 84th ed.; CRC Press: Boca Raton, 2003.

(42) Wolters, L. P.; Bickelhaupt, F. M. Halogen Bonding Versus Hydrogen Bonding: A Molecular Orbital Perspective. *ChemistryOpen* **2012**, *1*, 96−105.